Reduced dimension rovibrational variational calculations of the S1 state of C2H2. II. The S1 rovibrational manifold and the effects of isomerization

P. Bryan Changala, Joshua H. Baraban, John F. Stanton, Anthony J. Merer, and Robert W. Field

Citation: The Journal of Chemical Physics **140**, 024313 (2014); doi: 10.1063/1.4859876
View online: http://dx.doi.org/10.1063/1.4859876
View Table of Contents: http://scitation.aip.org/content/aip/journal/jcp/140/2?ver=pdfcov
Published by the AIP Publishing

Reduced dimension rovibrational variational calculations of the S_1 state of C_2H_2. II. The S_1 rovibrational manifold and the effects of isomerization

P. Bryan Changala,[1,a)] Joshua H. Baraban,[1,b)] John F. Stanton,[2] Anthony J. Merer,[3] and Robert W. Field[1]

[1]*Department of Chemistry, Massachusetts Institute of Technology, Cambridge, Massachusetts 02139, USA*
[2]*Department of Chemistry and Biochemistry, Institute for Theoretical Chemistry, The University of Texas at Austin, Austin, Texas 78712, USA*
[3]*Institute of Atomic and Molecular Sciences, Academia Sinica, Taipei 10617, Taiwan and Department of Chemistry, University of British Columbia, Vancouver, British Columbia V6T 1Z1, Canada*

(Received 22 October 2013; accepted 12 December 2013; published online 13 January 2014)

Reduced dimension variational calculations have been performed for the rovibrational level structure of the S_1 state of acetylene. The state exhibits an unusually complicated level structure, for various reasons. First, the potential energy surface has two accessible conformers, *trans* and *cis*. The *cis* conformer lies about 2700 cm^{-1} above the *trans*, and the barrier to *cis-trans* isomerization lies about 5000 cm^{-1} above the *trans* minimum. The *trans* vibrations ν_4 (torsion) and ν_6 (asym. bend) interact very strongly by Darling-Dennison and Coriolis resonances, such that their combination levels and overtones form polyads with unexpected structures. Both conformers exhibit very large x_{36} cross-anharmonicity since the pathway to isomerization is a combination of ν_6 and ν_3 (sym. bend). Near the isomerization barrier, the vibrational levels show an even-odd *K*-staggering of their rotational levels as a result of quantum mechanical tunneling through the barrier. The present calculations address all of these complications, and reproduce the observed *K*-structures of the bending and C–C stretching levels with good qualitative accuracy. It is expected that they will assist with the assignment of the irregular patterns near the isomerization barrier. © *2014 AIP Publishing LLC*. [http://dx.doi.org/10.1063/1.4859876]

I. INTRODUCTION

Few excited electronic states of polyatomic molecules have been as extensively studied as the S_1 ($\tilde{A}\,^1A_u$) state of acetylene, C_2H_2. Several decades of spectroscopy performed by many workers,[1–14] as well as numerous theoretical studies,[15–34] have shown that the molecule is *trans*-bent, and have given a complete vibrational assignment up to 4500 cm^{-1} of vibrational energy. A second conformer, where the molecule is *cis*-bent, was discovered recently.[13] It lies 2670 ± 10 cm^{-1} above the *trans* conformer,[34] and the barrier to isomerization is estimated to lie 4979 cm^{-1} (plus or minus a few hundred cm^{-1}) above the *trans* minimum.[33] Since the S_1-*cis* state transforms as A_2 in the C_{2v} point group, transitions to it from the Σ_g^+ electronic ground state are dipole-forbidden.

The primary complication of the *trans* manifold's rovibrational structure is the interaction between the nearly degenerate modes ν_4 (torsion) and ν_6 (asym. bend). These modes interact via Darling-Dennison resonance[11,35] and both *a*- and *b*-axis Coriolis coupling.[7] The result of these interactions is that the group of states with quantum numbers $v_4 + v_6 = n$ forms a bending polyad, abbreviated B^n. The bending polyads in *trans* C_2H_2 have been quite successfully modeled by effective Hamiltonian treatments,[11,12,14] in which the interaction parameters from high energy polyads scale in simple ways with those of low energy polyads, enabling a bootstrapped procedure of predicting high energy polyad structures from empirical fits of simpler low energy polyads. As nearly every vibrational level in the *trans* manifold belongs to a polyad, the robustness of the polyad patterns has been essential to successfully assigning the spectra of the S_1 state.

It is now known, however, that the addition of quanta of ν_3 (sym. bend) to *trans* bending polyads progressively breaks apart and eventually destroys the polyad structure because of the large x_{36} cross anharmonicity associated with the approach to the half-linear isomerization transition state.[12,14,34] The existence of a saddle point in the potential energy surface tests the limits of effective Hamiltonian treatments rooted in the assumption that the potential energy surface supports just one minimum and can be accurately represented as a relatively low-order power series expansion in the coordinates. Such difficulties have been noted before, for example, in Jacobson and Child's semiempirical, semiclassical inversion model of large amplitude motion in HCP,[36] and in Barnes and Kellman's approach to the isomerization in HO_2.[37,38] Though new empirical methods[39] have been proposed to model the multi-mode vibrational level structure resulting from the existence of a saddle point, an *ab initio* calculation that predicts the global rovibrational energy level structure and the associated wavefunctions is particularly useful for understanding both the physical nature and spectroscopic details of the emergent patterns caused by the isomerization.

a)Email: bryan.changala@colorado.edu Present address: JILA, National Institute of Standards and Technology and University of Colorado; and Department of Physics, University of Colorado, Boulder, Colorado 80309-0440, USA.
b)Present address: Department of Chemistry and Biochemistry, University of Colorado, Boulder, Colorado 80309-0215, USA.

A further consequence of isomerization in the S_1 state is that *cis* vibrational levels appear weakly in the $\tilde{A} - \tilde{X}$ spectra via tunneling into the *trans* well. The identification and assignment of these states[13,14] has required parallel *ab initio* efforts.[33,34] Continuing to push the assignment threshold to higher energies, up to and beyond the barrier to isomerization, is an additional motivation for the calculations presented in this paper.

The most recent *ab initio* study of S_1 acetylene prior to these calculations is the second-order vibrational perturbation theory (VPT2) treatment performed by some of the authors of the present work.[34] Those calculations are realistically targeted to levels with two or fewer quanta of excitation. They achieved excellent agreement with experimental values, especially for stretching modes, but they performed much more poorly for the low energy bending modes. As Section IV of that reference shows in detail, the difficulty can be traced to the implicit use of rectilinear coordinates. In contrast, the use of curvilinear coordinates in a variational calculation provides for a much more accurate treatment of such motions.

Finally, it has been recently observed that barrier-proximal states, which can tunnel through the barrier to isomerization, exhibit a tunneling splitting in the form of *K*-staggering within their rotational manifolds.[13,14] Though group theory allows for the possibility of these staggerings,[40] their sign and magnitude cannot be easily predicted *a priori*. Understanding these staggerings and gaining a foothold on quantitative estimates of them is essential for continued progress in the study of S_1 C_2H_2.

This paper is the second of two parts. Paper I (Ref. 41) contains details of the methodology and implementation, and the reader is directed there for full documentation of the computational methods. Paper II presents our variational results. In Sec. II, we examine the predicted fundamental frequencies as a means of evaluating the quality of the calculations. In Sec. III, the structure of the *trans* bending polyads is explored, as well as the effects of isomerization on their structure. Section IV contains predictions regarding the *cis* vibrational manifold. Finally, in Sec. V, we discuss *K*-staggering and its effects on the S_1 rovibrational level structure.

II. FUNDAMENTAL FREQUENCIES

For the reader who has not read Paper I, the following information is necessary for interpreting the results:

- A reduced dimension approximation is made by freezing the two CH bond lengths (r_1 and r_2), while leaving free the CC bond length (r_3), the two CCH bending angles (β_1, β_2) and the torsional angle (α); these degrees of freedom span, to a good approximation, modes ν_2, ν_3, ν_4, and ν_6 of both *trans* and *cis* acetylene.
- Total molecular rotation is explicitly included, permitting the calculation of different *J* and *K* states.
- A multivalued internal coordinate system is employed, requiring the use of the $G_4^{(8)}$ extended complete nuclear permutation inversion (CNPI) symmetry group.[40]
- A constrained, analytic reduced dimension rovibrational kinetic energy operator (KEO) is used, which properly accounts for the frozen CH bond lengths.
- Using a basis contraction scheme, a (3+3)D bending-torsion-rotation calculation (3 vibrational and 3 rotational degrees of freedom) is performed first; the eigenfunctions from this calculation are used to form a direct product basis with CC stretch basis functions to perform a (4+3)D calculation.

The sizes of the basis sets of each symmetry-*J* block of the rovibrational Hamiltonian were given in Table III of Paper I. The absolute convergence error of the lowest eigenvalues of these basis sets is <0.1 cm^{-1}. Relative energies are converged to perhaps another order of magnitude. For the highest states of interest, lying around 5000 cm^{-1} above the *trans* zero-point energy, the absolute convergence errors are of the order of 1 cm^{-1}.

As a means of evaluating the quality of our potential surface and the accuracy of our methods, we compare the observed and calculated fundamental frequencies for the *trans* and *cis* conformers in Table I. Only the modes approximately spanned in our reduced dimension internal coordinate space (ν_2, ν_3, ν_4, and ν_6 of each conformer) are included. Rough values are available for all of the *cis* frequencies, except ν_2. For it we list the vibrational fundamental as given by VPT2 anharmonic force field calculations.[34]

Examining modes of the *trans* conformer, for which all fundamentals are experimentally measured, it is clear that the 3D bending-torsion-rotation calculation is sufficient to describe the low frequency bends (ν_4 and ν_6), but fails to accurately reproduce the symmetric bending mode, ν_3. The residual for this mode is significantly reduced by the addition of the r_3 stretch in the 4D calculation, which is consistent with

TABLE I. Observed and calculated *trans* and *cis* fundamental frequencies. All values are in cm^{-1}. Three calculated columns are included: the initial 3D bending-torsion-rotation calculation (left), a 4D calculation including r_3 using the unconstrained KEO (center), and a 4D calculation using a correctly constrained KEO for frozen r_{CH} bond lengths (right).

Mode	Obs.	3D	4D w/ unconstrained KEO	4D w/ constrained KEO
trans				
ν_2 (r_{CC} stretch)	1387[a]	...	1443	1387
ν_3 (sym. bend)	1048[a]	1109	1074	1071
ν_4 (torsion)	765[b]	764	762[c]	749
ν_6 (asym. bend)	768[b]	770	769[c]	774
cis				
ν_2 (r_{CC} stretch)	(1503[d])	...	1595	1514
ν_3 (sym. bend)	740 ± 10[e]	783	776	764
ν_4 (torsion)	865 ± 10[e]	865	861[c]	844
ν_6 (asym. bend)	622[e,f]	618	615[c]	593

[a]Reference 3.
[b]Reference 7.
[c]These "4D" values for ν_4 and ν_6 were calculated on a 3D grid adiabatized along the r_3 coordinate.
[d]This fundamental has not been observed. We instead quote recent VPT2 calculations (Ref. 34) for comparison.
[e]Reference 13.
[f]Estimated from the $2\nu_6$ frequency divided by 2.

normal mode analyses that demonstrate a non-negligible contribution of r_3 displacement to ν_3. The ν_4 and ν_6 predictions indicate that our calculated potential energy surface is of sufficiently high quality to generate spectroscopic accuracy (a few cm^{-1}) even for an excited electronic state. The fact that these predictions worsen in the 4D calculation is possibly a result of the coarser grid point sampling of the 4D potential surface (as detailed in Paper I), but we cannot entirely rule out that it is an artifact of the constrained KEO.

The CC stretching mode ν_2 treated with an unconstrained KEO shows a considerably large residual. This may be at first unexpected as ν_2 is spanned almost exclusively by r_3 and therefore the current dimension reduction should treat this mode adequately. The source of the discrepancy, however, can be traced to the use of an unconstrained, full dimensional KEO. As is often done when using a full dimensional KEO in a reduced dimension calculation, the only change made to the KEO is to ignore terms with derivatives with respect to frozen coordinates (in this case the two r_{CH} bond lengths). We expect the kinetic energy of the r_3 stretch to be determined largely by the KEO term containing its second derivative, which, in the unconstrained KEO, is

$$\frac{-\hbar^2}{2}\frac{1}{\mu_{\text{CC}}}\frac{\partial^2}{\partial r_3^2}. \tag{1}$$

This expression indicates that the effective reduced mass of the r_3 stretch is equal to μ_{CC}, i.e., the unconstrained KEO treats the r_3 stretch as that between two carbon atom masses, as opposed to two CH fragments, which is intuitively what one would expect. In fact, replacing the C–C reduced mass, $\mu_{\text{CC}} = m_{\text{C}}/2$, with a CH dimer reduced mass, $\mu_{\text{CH,CH}} = (m_{\text{C}} + m_{\text{H}})/2 \approx (13/12)\mu_{\text{CC}}$, should lower the stretch frequency by $\sim\sqrt{12/13}$. Scaling the calculated unconstrained KEO frequency of 1443 cm^{-1} by this ratio yields 1386 cm^{-1}, almost exactly the observed ν_2 frequency. This suggests that, indeed, the unconstrained KEO incorrectly treats reduced masses (among other details) when naïvely applied to reduced dimension systems. The corresponding second derivative term in the constrained KEO (see the Appendix of Paper I) equals

$$\frac{-\hbar^2}{2}\left[\frac{1}{\mu_{\text{CC}}} - \frac{\mu_{\text{CH}}}{m_C^2}(\cos^2\beta_1 + \cos^2\beta_2)\right]\frac{\partial^2}{\partial r_3^2}. \tag{2}$$

The effective r_3 stretching mass is geometry-dependent according to the middle factor of the above expression. At linear geometries ($\beta_1 = \beta_2 = 0$), the mass factor is exactly the inverse CH dimer reduced mass, as expected. When $\beta_1 = \beta_2 = 90^\circ$, both cosine terms are zero and the effective mass is that of two carbon atoms. At other geometries, the effective mass equals some intermediate value.

The calculated *trans* fundamental frequencies using the constrained KEO are shown in the right-most column of Table I. The ν_2 frequency clearly improves, matching the observed value to less than 1 cm^{-1}, demonstrating the necessity of a properly constrained reduced dimension KEO, as discussed in Paper I. The low frequency bends, ν_4 and ν_6, actually worsen. As mentioned above, this is likely due to the more sparsely sampled 4D PES grid. It will be seen, however, that these small errors in the fundamental frequencies have relatively little effect on the calculated local polyad structures of high lying overtones and combination bands of ν_4 and ν_6.

The *cis* fundamental frequency predictions behave in a similar way to those of the *trans* conformer. ν_4 and ν_6 are expected to be the most accurate of the 3D calculation. In fact, ν_4 is in perfect agreement with the experimentally observed value, and the ν_6 frequency is reproduced quite well, within 1% error. For the same reason as above, the *cis* ν_3 fundamental frequency in the 3D calculation is overestimated. The 4D calculation shows a similar degradation of the ν_4 and ν_6 frequencies. The ν_3 frequency improves with the inclusion of r_3 displacement, while the ν_2 frequency with the constrained KEO is in relatively good agreement with the VPT2 prediction.[34] At least some of the current *cis* predictions' discrepancies can be attributed to the fact that the PES was calculated with CH bond lengths constrained to their *trans* equilibrium values, $r_{\text{CH}} = 1.0963$ Å, which is about 0.2% smaller than the *cis* equilibrium value, $r_{\text{CH}} = 1.0983$ Å.[33]

III. BENDING POLYADS AND THE ONSET OF ISOMERIZATION

A complete $J = K = 0$ level list of predicted vibrational states with assignments from the *trans* origin to 5000 cm^{-1} of internal energy is included in the Appendix. It would be both tedious and mostly uninformative to compare the calculated structure to the observed levels state-by-state; instead, we examine specific representative cases.

An overview diagram of the observed and calculated *trans* and *cis* $J = 0$ level structure is shown in Figure 1.

Apart from the slight overestimation of the ν_3 frequency, the overtones and combination bands involving ν_2 and ν_3 are reproduced quite well (left side of Figure 1). These levels display very little interesting structure and conform to simple anharmonic oscillator energy level patterns.

The first challenge for *ab initio* calculations involves the overtones of modes ν_4 and ν_6. Errors in the calculated bending fundamental frequencies, as discussed above, lead to some clearly-seen systematic offsets of the higher lying bending polyads. However, the *internal* structure of each polyad is reproduced with impressive accuracy. Figure 2 shows the observed and calculated (4D) $J = K = 0$–2 level structure of B^4, the polyad containing the zero-order $\{4^4, 4^3 6^1, 4^2 6^2, 4^1 6^3, 6^4\}$ vibrational states. Overall, the complicated course of the perturbed asymmetric top levels is well reproduced, despite the small discrepancies in the ν_4 and ν_6 fundamental frequencies. After correcting for the net offset of the calculated polyad, the intrapolyad structure has a rms residual of only 4.9 cm^{-1}. Other calculated polyads throughout the *trans* manifold have similar intrapolyad structure rms residuals. These residuals are about the same as those of effective Hamiltonian models that use interaction parameters from lower energy polyads to predict the structure of higher lying levels.

Variational eigenfunctions provide important insight into the physical nature of rovibrational dynamics. One notable result of polyad effective Hamiltonians in *trans* acetylene is that the polyad members possess approximate vibrational angular momentum.[11] Inspection of the variational wavefunctions for the B^4 polyad elaborated upon in the preceding paragraph

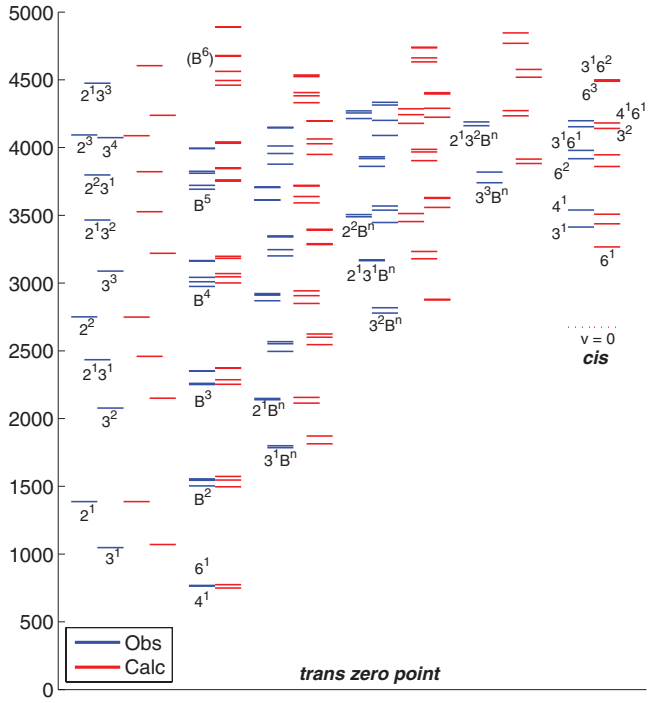

FIG. 1. Observed and calculated S_1 vibrational levels (energies in cm^{-1}). $J = 0$ vibrational energies are shown for almost all vibrational levels under 5000 cm^{-1} of internal energy. Assigned observed levels are shown in blue (left side of each stack). Calculated levels are in red (right side of each stack). All levels are *trans* except for the rightmost column labeled "*cis*." An offset of 240 cm^{-1} was subtracted from the calculated *cis* levels such that the calculated and empirically estimated value of the *cis* $v = 0$ origin (2670 $\pm$ 10 cm^{-1}, Ref. 34) coincide. The *cis* origin is indicated with a dashed line, as it remains unobserved.

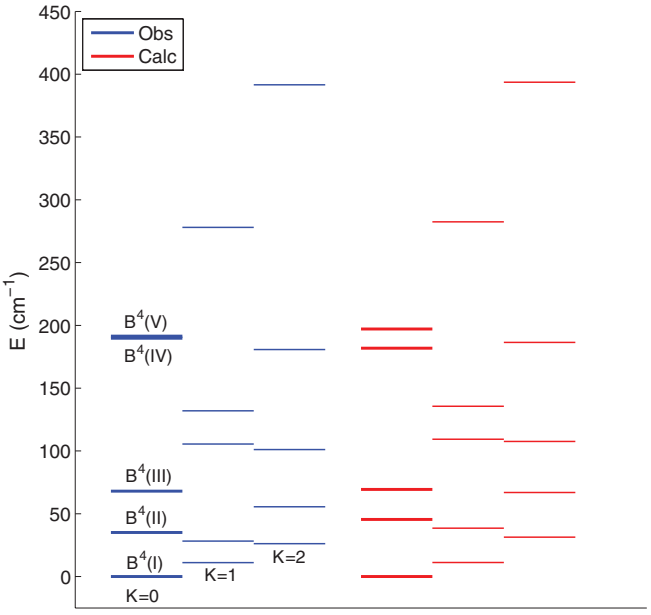

FIG. 2. Observed (blue, left) and calculated (red, right) $J = K = 0$–2 levels of the B^4 polyad, which contains five vibrational members. Only eight of the 15 expected K-stacks with $K = 0$–2 have been assigned. For unassigned states, calculated values based on parameters from lower bending polyads are given (Ref. 11). Bold lines indicate $J = K = 0$ levels, which are the same as those shown for this polyad in Figure 1. The "center of gravity" of the polyad has been subtracted to compare only the *intrapolyad* structure, ignoring systematic offsets. The bending polyads deviate significantly from the normal $E \propto K^2$ prolate top rotational energy level pattern. Despite the fact that the $J = K = 0$–2 levels span 400 cm^{-1}, the 4D calculated structure has an rms residual of only 4.9 cm^{-1}.

clearly confirms such an interpretation, as is illustrated in Figure 3.

As discussed above, effective Hamiltonian models begin to break down for 3^m6^n combination levels because of the large x_{36} cross anharmonicity associated with the approach to the barrier to isomerization.[12,14] Prior reduced dimension discrete variable representation (DVR) vibrational calculations of the S_1 state[33] have shown that such levels are increasingly delocalized across the *cis-trans* isomerization barrier. This work, by including the torsional degree of freedom, extends this result by enabling an examination of the wavefunctions for all states of 3^mB^n polyads, among which isomerizing states are especially interesting. Figure 4 compares the $\{\beta_1, \beta_2, \alpha\}$ projections of the wavefunctions of B^4, 3^1B^4, and 3^2B^4 polyads as given by the 4D calculation. As a reminder, β_1 and β_2 are CCH bending angles and α is the torsional out-of-plane angle (see Paper I). For the pure bending polyad, B^4, the coupled vibrational angular momentum structure is the same as that seen in Figure 3. The addition of one or two quanta of ν_3 begins to alter the polyad coupling patterns. The lowest member is decoupled from the remainder of the polyad. This selective and incremental decoupling can be seen in the loss of vibrational angular momentum structure in the wavefunction and the onset of delocalization into the *cis* well, especially for 3^26^4 in the lower left plot of the figure. This decoupling is associated with the large cross-anharmonicity of ν_3 and ν_6. The predicted magnitude of the (negative) cross-anharmonicity in this calculation is smaller than experimentally observed (for example, we predict 3^16^1 to lie, erroneously, above 3^14^1); however, the general pattern of 3^n6^m combination bands is still well reproduced.

Our accurate calculation of polyad structures will be an important tool in understanding spectra of the S_1 state immediately below the barrier to isomerization. Polyad structures

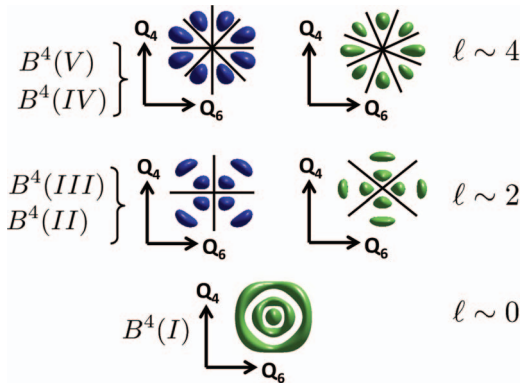

FIG. 3. Variational wavefunctions of the B^4 polyad ($|\Psi|^2$ is plotted). The coupling between modes ν_4 and ν_6 is manifest. The angular nodal patterns (shown with solid lines) are consistent with the expected vibrational angular momentum generated in the bending polyads and allow the polyad members to be organized with an approximate vibrational angular momentum quantum number $\ell \approx 0, 2, 4$. Member states of B^4 are labeled in absolute energy order by Roman numerals.

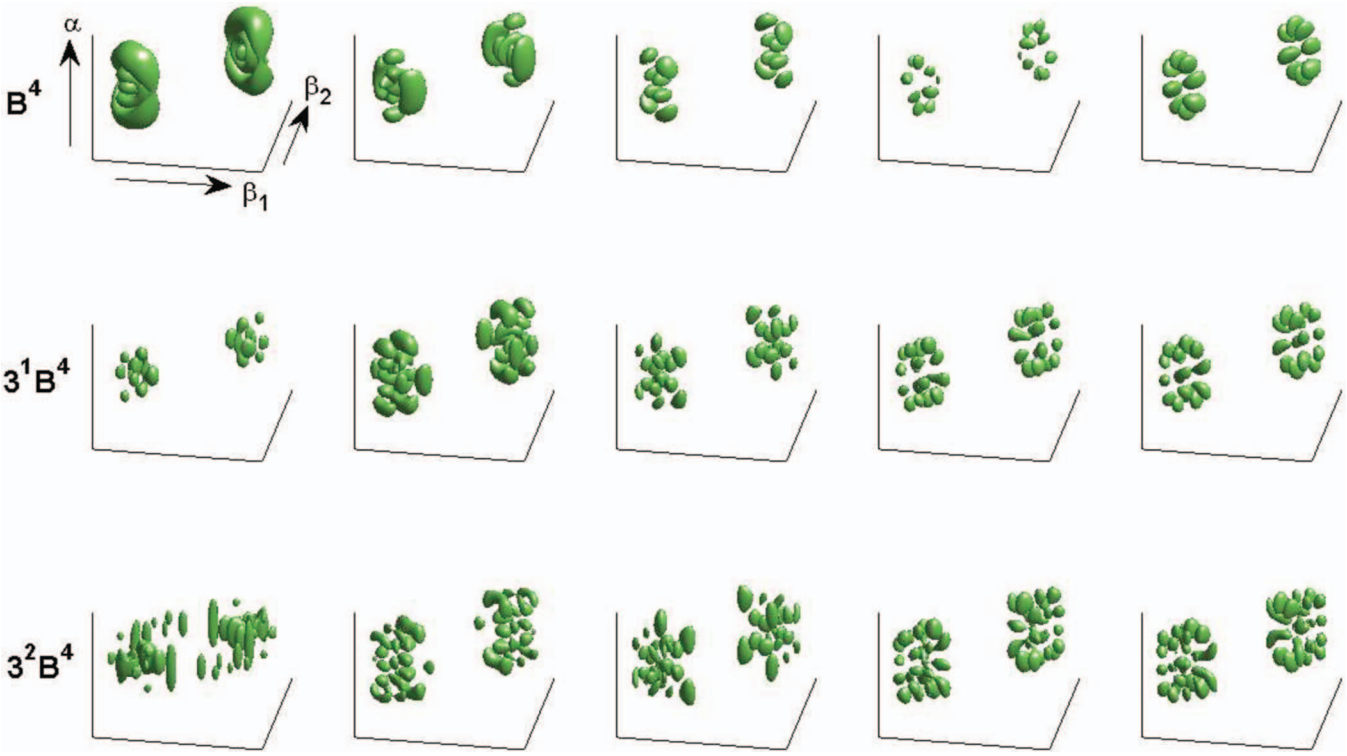

FIG. 4. Decoupling of the 3^nB^4 polyads. The bending-torsion projections of 4D, $J = 0$ wavefunctions for the B^4, 3^1B^4, and 3^2B^4 polyads are shown in the first, second, and third rows, respectively. Isosurfaces of the squared amplitude ($|\Psi|^2$) are plotted. The lowest energy polyad member is on the far left of each row. As v_3 increases, the lowest member of the polyad becomes decoupled from the rest of the polyad, restoring its nominal 3^n6^4 character. 3^26^4 (lowest left-most wavefunction) exhibits *cis-trans* delocalization and tunneling through the isomerization barrier.

broken apart by the effects of isomerization are difficult to predict with effective Hamiltonian models. Variational treatments generate the complete rovibrational manifold in a single calculation and thus allow us to understand—both globally and in detail—the patterns of the rovibrational structure of isomerizing systems.

IV. *cis* VIBRATIONAL MANIFOLD

The vibrational assignments of the experimentally observed *cis* states[13,14] have been guided to some extent by *ab initio* calculations[33,34] of *cis* vibrational frequencies. Completing the identification and assignment of the remaining *cis* vibrational levels below and near the barrier to isomerization will undoubtedly benefit from continued theoretical studies. We summarize in Table II the observed and calculated positions of the low energy *cis* vibrational manifold. Despite residuals of tens of cm^{-1} in the variational results, the level structure is sufficiently sparse to confirm the vibrational assignments with confidence. It should be noted that the variational PES was optimized for *trans* geometries (i.e., *trans* r_{CH} bond lengths), which results in systematically larger residuals for the *cis* predictions than for the *trans*. As mentioned above, the residuals in the variational predictions for the *cis* frequencies are expected to improve if a finer PES grid spacing is used around the equilibrium configuration, as well as allowing for relaxation of the CH distances.

V. K-STAGGERING AND TUNNELING INTERACTIONS

For any molecule with low barriers between local equilibrium geometries, barrier crossings and tunneling interactions will have an important qualitative impact on barrier-proximal states and their level structure. S_1 C_2H_2 is an especially interesting case in that there are both several non-equivalent wells

TABLE II. Observed and calculated positions of some low-lying *cis* vibrational levels. Observed levels are reported in Refs. 13 and 14. VPT2 calculations are second-order vibrational perturbation theory results from a full dimensional anharmonic force field (Ref. 34). All values are in cm^{-1} relative to the *cis* origin.

cis state	Obs.	Calc. (VPT2)	Calc. (this work)
$v = 0$	0[a]	0[a]	0
6^1	…	607[b]	593
3^1	740[a]	740[a]	764
4^1	865	865[b]	834
6^2	1244	1244[b]	1186
3^16^1	1305	1294[b]	1273
3^2	1477[a]	1476[a]	1509
2^1	…	1503	1514
4^16^1	1524	1535[b]	1467
3^14^1	…	1572[b]	1579
6^3	…	…	1815

[a]The *cis* zero point has not been observed. Its value is derived to be 44 870 ± 10 cm^{-1} based on the observation of *cis* 3^1 and 3^2 and the VPT2 calculation of *cis* x_{33}.
[b]These VPT2 values include an empirical correction of the v_4 and v_6 frequencies (see Ref. 34 for details).

(*cis* and *trans* conformers) and two conceivable isomerization pathways between these wells (i.e., in-plane bending involving a mixture of symmetric and asymmetric bending modes and out-of-plane torsion). Though such properties make *cis-trans* isomerization in acetylene a complicated problem, they create patterns that encode details about *cis-trans* interactions and the associated isomerization dynamics.

It is convenient to divide the energy region where *cis-trans* tunneling is important into two parts. The lower energy part includes states where the tunneling interaction energies are much smaller than the spacing between localized *cis* and *trans* vibrational levels. The upper energy part includes states near the top of the isomerization barrier where tunneling effects are no longer perturbative, and interactions between wells dominate the level structure. In reality, of course, there is a continuous distribution between these regimes, but this distinction will help frame the discussion of tunneling patterns.

The simplest tunneling case is an interaction between degenerate localized states in identical potential wells. Figure 5(a) shows a 2D contour plot of the S_1 PES for planar geometries ($\alpha = 0$). The axes correspond to the two CCH bond angles $\beta_{1,2}$. The upper right and lower left quadrants contain two equivalent *cis* wells, while the upper left and lower right are *trans*. We consider localized wavefunctions in the two *cis* wells, which interact to form symmetrized tunneling components: a symmetric and antisymmetric linear combination. In Figure 5(b), we show transformations that may be applied to such wavefunctions. For the symmetric tunneling component, moving from configuration (1) to (3) via in-plane bending (2) leaves the value of the wavefunction unchanged (with no sign change), while the wavefunction of the antisymmetric component acquires a negative sign. A 180° rotation about the body-fixed z-axis returns the molecule to the same space-fixed coordinates as (1), and therefore the total wavefunction *must* return to its original value. This implies that the rotational factor of the total wavefunction must undergo no sign change for symmetric tunneling components,

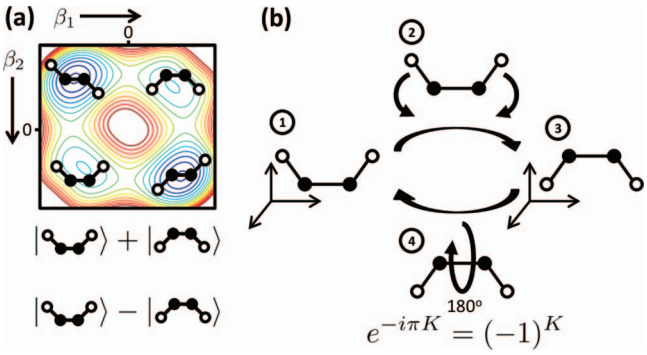

FIG. 5. Tunneling in *cis* vibrational states. (a) 2D in-plane bending potential with two equivalent *cis* and *trans* wells. Degenerate localized wavefunctions in each equivalent well form symmetric and antisymmetric tunneling linear combinations. (b) A molecule in the lower left *cis* well (1) can isomerize via in-plane bending (2) to an equivalent *cis* well (3), which can be transformed back to the original orientation via a 180° rotation about the CC-axis (4). The requirement of a single-valued wavefunction entails that symmetric tunneling components have only even K states and antisymmetric tunneling components have only odd K states.

but must acquire a negative sign for antisymmetric components. The phase change of such a rotation about the z-axis is $\exp(-i\pi K) = (-1)^K$. Thus symmetric tunneling components can only have rotational factors with even K and antisymmetric tunneling components can only have rotational factors with odd K. Tunneling splittings in acetylene will therefore appear as a staggering between the even and odd K levels of a vibrational state. This is distinct from how tunneling splittings appear in ammonia or methyl rotors.

The relevant extended CNPI group theory for treating isomerization in S_1 acetylene using the $G_4^{(8)}$ symmetry group is fully treated by Hougen and Merer in Ref. 40. It can be shown that nearest-neighbor tunneling interactions should lead to an even/odd K-staggering for in-plane isomerization. If torsional isomerization is feasible, then an additional staggering between $K = 4n$ and $K = 4n + 2$ states should occur.

A summary of observed and calculated staggerings is given in Table III. Because of the small number of observed *cis* levels and their respective K rotational manifolds, few K-staggering measurements have been reported for this conformer. It is difficult to determine K-staggerings in *trans* polyads because the strong a-axis Coriolis coupling distorts the structure. Some *trans* levels that are not parts of polyads, like high overtones of ν_3, are unaffected by such perturbations and have readily identifiable staggerings. For the two experimental *cis* data points available, the predictions agree in the direction and approximate magnitude of the K-staggering. The K-staggering for the *cis* origin level is predicted to be quite small and we anticipate that it will not be distinguishable from other factors affecting the rotational structure. Only one bending quantum higher than the levels where staggerings have been observed, the staggerings are predicted to be an order of magnitude larger (e.g., *cis* $3^1 6^2$ and 6^3). There are two related contributions to this trend. First, the simple tunneling interactions between degenerate vibrational states belonging to identical wells (i.e., *cis-cis* or *trans-trans* tunneling) become larger as the barrier is approached. Second, resonant interactions between nearby *cis* and *trans* states are introduced. Because the CNPI symmetries of the rotational levels depend on K, the possible *cis-trans* interactions are

TABLE III. K-staggerings in *cis* and *trans* vibrational states. Listed are the observed and calculated K-staggerings for several vibrational states. A positive staggering indicates the odd K levels appear higher in energy than expected from the positions of even K levels. All values are in cm^{-1}.

cis			*trans*		
State	Obs.	Calc.	State	Obs.	Calc.
$3^1 6^1$	$+3.9$[a]	$+1.6$[b]	3^4	(0)[c]	(0)
6^2	-5 ± 1[d]	-3.0[b]	3^5	$+6.3$[c]	-4.1[e]
$v = 0$	…	$+0.03$[b]	$3^4 6^1$	$+28$[f]	-19[b]
$3^1 6^2$	…	$+42$[b]	$3^4 6^2$	-6.9[f]	$+56$[e] (-64[b])
6^3	…	-62[b]			

[a]Reference 13.
[b]3D value.
[c]Reference 4.
[d]Reference 14.
[e]4D value.
[f]Our unpublished spectra with tentative assignments.

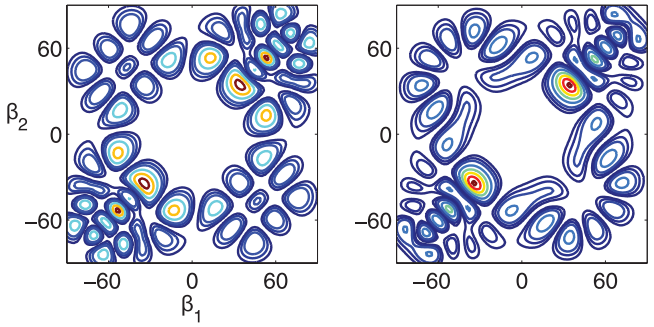

FIG. 6. *K*-dependent *cis-trans* interactions in *trans* $3^4 6^2$. This figure shows the calculated vibrational wavefunctions ($|\Psi|^2$) of the $K = 0$ (left) and $K = 1$ (right) states of *trans* $3^4 6^2$ in the $\alpha = 0$ plane (i.e., planar geometries). Both demonstrate significant *cis-trans* delocalization (the *trans* geometries are in the lower left and upper right quadrants and the *cis* geometries are in the upper left and lower right quadrants). The $K = 0$ component interacts with *cis* $3^2 6^2$, but the $K = 1$ component interacts with *cis* $3^3 6^1$. The *K* dependence of *cis-trans* tunneling leads to significant *K*-staggering for zero-order states with the same vibrational character.

different for even or odd *K*. This gives a further contribution to the *K*-staggering.

The patterns associated with this latter type of *cis-trans* staggering are expected to be less consistent, as the level shifts depend sensitively on the relative positions of near-resonant *cis* and *trans* states. Even within this calculation, the sign of the shift can change, as it does, for example, with the 3D and 4D *K*-staggering prediction for *trans* $3^4 6^2$, although the magnitude remains approximately the same. From a perturbation theory perspective, small *cis-cis* and *trans-trans* tunneling interactions between identical wells are a first-order effect, while *K*-dependent *cis-trans* interactions are a second-order effect.

It may be impossible to distinguish empirically between these two types of interactions in the observed spectra. However, in the variational wavefunctions, *K*-dependent *cis-trans* interactions are readily identified. As one example, the $\alpha = 0$ cross-section of the *trans* $3^4 6^2$ wavefunction, for which the magnitude of the *K*-staggering could be as large as 60 cm^{-1}, is shown in Figure 6. The figure shows the calculated vibrational wavefunctions for both the $K = 0$ and 1 rotational components. Both rotational components show extensive *cis-trans* delocalization. However, the $K = 0$ component interacts with *cis* $3^2 6^2$, and the $K = 1$ with *cis* $3^3 6^1$, leading to a large predicted staggering between even and odd *K* states. These asymmetric *cis-trans* interactions are especially sensitive to local resonances between the two wells, making it difficult for *ab initio* calculations to predict the detailed interactions between the uncorrelated zero-order structures of the *cis* and *trans* manifolds. However, these calculations provide qualitative patterns that are valuable when attempting to analyze spectra of the near-barrier region.

VI. CONCLUSIONS

In this paper, we have presented the highest dimension rovibrational variational calculations of S_1 acetylene to date. We have reproduced some of the most complicated aspects of this electronic state's rovibrational structure, which include the ν_4/ν_6 bending polyads, the effects of *cis-trans* isomerization on the level structure of $3^m 6^n$ combination bands, and the presence of *K*-staggering in levels that tunnel through barriers to isomerization. One strength of this variational treatment is that the entire global structure is generated with a single calculation, which allows patterns to be examined over large ranges of internal energy.

Though our calculations have contributed significantly to our understanding of *cis-trans* tunneling interactions, improving the quantitative accuracy of *K*-staggering predictions should be a primary goal of future theoretical studies of S_1 C_2H_2. The issue of sensitivity to local *cis-trans* level patterns may perhaps be overcome with a low dimension empirically fit effective potential, such as a 2D CCH bending model. However, it could very well be that a full dimensional treatment is required to obtain spectroscopically accurate predictions of *K*-staggerings.

In the Introduction, we alluded to an extended effective Hamiltonian approach to the isomerization of HO_2.[37,38] However, we are less hopeful that such a model could be developed for *cis-trans* isomerization in S_1 C_2H_2 due to a number of significant complications: (i) acetylene exhibits an essentially complete mixing of normal modes along the isomerization path, whereas HO_2, though requiring both stretch and bend excitation to isomerize, dominantly proceeds along the bending coordinate; (ii) acetylene contains other resonances, such as the coupling between *trans* ν_4 and ν_6, which are not directly involved with the isomerization but would need to be accounted for in an effective Hamiltonian, complicating any conceivable model; and (iii) perhaps most importantly, the *asymmetric* double minimum potential of S_1 acetylene is a qualitatively distinct and more difficult system than that of a symmetric double well potential.

Exclusive attention has been devoted in this paper to the calculated rovibrational structure below and up to the barrier to isomerization. These calculations, of course, give predictions for the structure above the barrier as well. This predicted structure, however, has yet to be analyzed. Qualitatively new level patterns will emerge resulting from unhindered large amplitude internal motions. Among these is the development of approximate vibrational angular momentum about the out-of-plane (*c*) axis. *Ab initio* calculations conducted in parallel with the analysis of high energy spectra will certainly prove necessary in order to understand the undoubtedly complicated level structure of such energy regions.

ACKNOWLEDGMENTS

P.B.C., J.H.B., and R.W.F. acknowledge support of this work at MIT by U.S. Department of Energy Grant No. DE-FG0287ER13671. P.B.C. would like to thank Stephen Neushul of iCRco, Inc. for the use of workstation computing time, Jon Hougen for stimulating discussions, and the MIT Undergraduate Research Opportunities Program for support.

APPENDIX: $J = K = 0$ LEVEL LIST

See Table IV.

TABLE IV. Calculated 4D $J = K = 0$ level list. Assignments for all vibrational states up to 5000 cm^{-1} above the *trans* zero point are included. States are organized by their $G_4^{(8)}$ symmetry (with correlations to C_{2h} and C_{2v} labels provided). *trans* states are labeled by quantum numbers only. *cis* states are prefixed explicitly by "*cis*." Local interactions which mix zero-order states of the same symmetry are indicated by superscript letters prefixed to the vibrational assignment.

	A_{1g}^+ (A_g, A_1)		A_{2g}^- (B_g, B_1)		B_{2u}^+ (B_u, B_2)		B_{1u}^- (A_u, A_2)	
0	0	0.000	$4^1 6^1$	1546.190	6^1	774.087	4^1	748.972
1	3^1	1070.776	$3^1 4^1 6^1$	2624.276	$3^1 6^1$	1871.176	$3^1 4^1$	1813.488
2	2^1	1386.935	$2^1 4^1 6^1$	2907.211	$2^1 6^1$	2155.751	$2^1 4^1$	2113.802
3	$B^2(4^2)$	1496.216	B^4	3046.354	B^3	2286.898	B^3	2253.305
4	$B^2(6^2)$	1573.437	B^4	3197.974	B^3	2373.155	B^3	2370.655
5	3^2	2150.114	$3^2 4^1 6^1$	3625.150	$3^2 6^1$	2880.419	$3^2 4^1$	2875.804
6	$2^1 3^1$	2459.348	$2^1 3^1 4^1 6^1$	3967.769	$2^1 3^1 6^1$	3233.536	$2^1 3^1 4^1$	3179.374
7	$3^1 B^2$	2545.400	$3^1 B^4$	4027.964	$3^1 6^3$	3283.891	$3^1 B^3$	3290.462
8	$3^1 B^2$	2600.272	$3^1 B^4$	4197.186	$3^1 B^3$	3397.171	$3^1 B^3$	3390.403
9	2^2	2749.267	$2^2 4^1 6^1$	4242.738	$cis\,6^1$	3506.727	$2^2 4^1$	3453.282
10	$2^1 4^2$	2849.488	$^a cis\,4^1 6^1$	4380.575	$2^2 6^1$	3512.657	$2^1 B^3$	3591.764
11	$cis\,0$	2913.603	$^a 2^1 B^4$	4382.426	$2^1 B^3$	3638.571	$2^1 B^3$	3716.241
12	$2^1 6^2$	2942.205	B^6	4495.158	$2^1 B^3$	3721.625	$cis\,4^1$	3747.777
13	B^4	3000.878	$2^1 B^4$	4535.566	B^5	3761.452	B^5	3752.188
14	B^4	3070.299	$3^3 4^1 6^1$	4605.019	$^a B^5$	3844.902	B^5	3849.977
15	B^4	3182.692	B^6	4679.541	$^a 3^3 6^1$	3882.260	$3^3 4^1$	3914.903
16	3^3	3219.905	B^6	4888.737	B^5	4032.311	B^5	4041.770
17	$^a 2^1 3^2$	3526.528	$3^2 B^4$	4947.392	$^b cis\,3^1 6^1$	4186.718	$2^1 3^2 4^1$	4234.222
18	$^a 3^2 6^2$	3557.865	$2^1 3^2 4^1 6^1$	4994.302	$^b 3^2 6^3$	4223.249	$3^2 B^3$	4289.494
19	$3^2 4^2$	3631.286	$cis\,3^1 4^1 6^1$	5078.797	$2^1 3^2 6^1$	4272.160	$3^2 B^3$	4404.902
20	$cis\,3^1$	3677.482	$3^2 B^4$	5188.374	$3^2 B^3$	4395.006	$cis\,3^1 4^1$	4492.842
21	$2^2 3^1$	3822.057	$^b 2^2 3^1 4^1 6^1$	5289.706	$2^2 3^1 6^1$	4576.649	$2^2 3^1 4^1$	4519.321
22	$2^1 3^1 4^2$	3903.132	$^b 2^1 3^1 B^4$	5361.199	$^c 3^1 B^5$	4615.540	$2^1 3^1 B^3$	4632.681
23	$^b 3^1 B^4$	3949.312	$^b 3^1 B^6$	5403.682	$^c 2^1 3^1 6^3$	4662.041	$3^1 B^5$	4709.051
24	$^b 2^1 3^1 6^2$	3986.884	$2^1 3^1 B^4$	5524.929	$cis\,6^3$	4729.097	$2^1 3^1 B^3$	4740.926
25	$3^1 B^4$	4064.047	$2^3 4^1 6^1$	5555.472	$2^1 3^1 B^3$	4736.278	$2^3 4^1$	4769.802
26	2^3	4087.331	$3^4 4^1 6^1$	5561.245	$^d 3^4 6^1$	4806.953	$3^1 B^5$	4851.845
27	$cis\,6^2$	4099.394	$^d 3^1 B^6$	5604.622	$^d 3^1 B^5$	4824.154	$2^2 B^3$	4905.418
28	$2^2 4^2$	4178.966	$^d cis\,4^1 6^3$	5647.290	$2^3 6^1$	4845.775	$3^4 4^1$	4933.373
29	$3^1 B^4$	4196.799	$2^2 B^4$	5692.860	$cis\,3^2 6^1$	4914.631	$cis\,4^1 6^2$	5007.470
30	3^4	4238.469	$cis\,3^2 4^1 6^1$	5765.880	$2^2 B^3$	4965.660	$3^1 B^5$	5023.834
31	$2^2 6^2$	4286.130	$2^1 B^6$	5812.286	$cis\,2^1 6^1$	5001.845		5038.916
32	$2^1 B^4$	4330.680	$2^2 B^4$	5848.320	$3^1 B^5$	5019.101		5070.587
33	$2^1 B^4$	4405.469	$cis\,2^1 4^1 6^1$	5849.811	$2^2 B^3$	5049.488		5161.822
34	$cis\,3^2$	4422.134	$3^1 B^6$	5870.068		5079.659		5195.072
35	$cis\,2^1$	4427.577		5900.103		5103.546		5222.683
36	B^6	4460.850		5943.805		5190.127		5234.761
37	$^c 3^3 6^2$	4500.656		5967.844		5207.753		5253.869
38	$^c 2^1 B^4$	4523.688		6008.429		5258.506		5278.967
39	B^6	4562.393		6116.252		5281.146		5340.651
40	$2^1 3^3$	4604.597		6146.192		5303.949		5371.979
41	$cis\,4^2$	4631.747		6191.554		5347.931		5393.805
42	$3^3 4^2$	4641.684		6198.328		5358.627		5506.149
43	B^6	4675.332		6238.396		5392.043		5528.228
44	$cis\,3^1 6^2$	4739.798		6284.169		5512.369		5560.690
45	$^d 2^2 3^2$	4876.914		6346.790		5552.030		5569.917
46	B^6	4888.964		6365.483		5575.132		5645.486
47	$^d 3^2 B^4$	4899.278		6395.413		5591.149		5733.545
48	$^d 2^1 3^2 B^2$	4941.710		6419.677		5641.904		5741.453
49	$^d 2^1 3^2 B^2$	4985.308		6513.885		5696.065		5755.534
50	$3^2 B^4$	5048.903		6521.398		5721.317		5826.315

[1]C. K. Ingold and G. W. King, J. Chem. Soc. **1953**, 2702 (1953).
[2]K. K. Innes, J. Chem. Phys. **22**, 863 (1954).
[3]J. K. G. Watson, M. Herman, J. C. Van Craen, and R. Colin, J. Mol. Spectrosc. **95**, 101 (1982).
[4]J. C. Van Craen, M. Herman, R. Colin, and J. K. G. Watson, J. Mol. Spectrosc. **111**, 185 (1985).
[5]J. C. Van Craen, M. Herman, R. Colin, and J. K. G. Watson, J. Mol. Spectrosc. **119**, 137 (1986).
[6]J. D. Tobiason, A. L. Utz, and F. F. Crim, J. Chem. Phys. **99**, 928 (1993).
[7]A. L. Utz, J. D. Tobiason, E. Carrasquillo M., L. J. Sanders, and F. F. Crim, J. Chem. Phys. **98**, 2742 (1993).
[8]M. Mizoguchi, N. Yamakita, S. Tsuchiya, A. Iwasaki, K. Hoshina, and K. Yamanouchi, J. Phys. Chem. A **104**, 10212 (2000).
[9]A. J. Merer, N. Yamakita, S. Tsuchiya, J. F. Stanton, Z. Duan, and R. W. Field, Mol. Phys. **101**, 663 (2003).
[10]A. H. Steeves, A. J. Merer, H. A. Bechtel, A. R. Beck, and R. W. Field, Mol. Phys. **106**, 1867 (2008).
[11]A. J. Merer, N. Yamakita, S. Tsuchiya, A. H. Steeves, H. A. Bechtel, and R. W. Field, J. Chem. Phys. **129**, 054304 (2008).
[12]A. H. Steeves, H. A. Bechtel, A. J. Merer, N. Yamakita, S. Tsuchiya, and R. W. Field, J. Mol. Spectrosc. **256**, 256 (2009).
[13]A. J. Merer, A. H. Steeves, J. H. Baraban, H. A. Bechtel, and R. W. Field, J. Chem. Phys. **134**, 244310 (2011).
[14]J. H. Baraban, P. B. Changala, A. J. Merer, A. H. Steeves, H. A. Bechtel, and R. W. Field, Mol. Phys. **110**, 2707 (2012).
[15]I. G. Ross, Trans. Faraday Soc. **48**, 973 (1952).
[16]A. D. Walsh, J. Chem. Soc. **1953**, 2288 (1953).
[17]R. S. Mulliken, Can. J. Chem. **36**, 10 (1958).
[18]H. Howard and G. W. King, Can. J. Chem. **37**, 700 (1959).
[19]W. E. Kammer, Chem. Phys. Lett. **6**, 529 (1970).
[20]W. E. Kammer, Chem. Phys. **5**, 408 (1974).
[21]D. Demoulin and M. Jungen, Theor. Chim. Acta **34**, 1 (1974).
[22]D. Demoulin, Chem. Phys. **11**, 329 (1975).
[23]S. P. So, R. W. Wetmore, and H. F. Schaefer, J. Chem. Phys. **73**, 5706 (1980).
[24]M. Perić, R. J. Buenker, and S. D. Peyerimhoff, Mol. Phys. **53**, 1177 (1984).
[25]H. Lischka and A. Karpfen, Chem. Phys. **102**, 77 (1986).
[26]Y. Osamura, F. Mitsuhashi, and S. Iwata, Chem. Phys. Lett. **164**, 205 (1989).
[27]J. F. Stanton, C.-M. Huang, and P. G. Szalay, J. Chem. Phys. **101**, 356 (1994).
[28]K. Malsch, R. Rebentisch, P. Swiderek, and G. Hohlneicher, Theor. Chem. Acc. **100**, 171 (1998).
[29]K. Malsch, G. Hohlneicher, R. Schork, and H. Köppel, Phys. Chem. Chem. Phys. **3**, 5393 (2001).
[30]E. Ventura, M. Dallos, and H. Lischka, J. Chem. Phys. **118**, 1702 (2003).
[31]M. Kállay and J. Gauss, J. Chem. Phys. **121**, 9257 (2004).
[32]B. Schubert, H. Köppel, and H. Lischka, J. Chem. Phys. **122**, 184312 (2005).
[33]J. H. Baraban, A. R. Beck, A. H. Steeves, J. F. Stanton, and R. W. Field, J. Chem. Phys. **134**, 244311 (2011).
[34]J. H. Baraban, J. F. Stanton, A. J. Merer, and R. W. Field, Mol. Phys. **110**, 2725 (2012).
[35]B. T. Darling and D. M. Dennison, Phys. Rev. **57**, 128 (1940).
[36]M. P. Jacobson and M. S. Child, J. Chem. Phys. **114**, 262 (2001).
[37]G. Barnes and M. Kellman, J. Chem. Phys. **133**, 101105 (2010).
[38]G. Barnes and M. Kellman, J. Chem. Phys. **134**, 074108 (2011).
[39]J. H. Baraban, P. B. Changala, A. J. Merer, and R. W. Field, "Spectroscopic characterization of transition states" (unpublished).
[40]J. T. Hougen and A. J. Merer, J. Mol. Spectrosc. **267**, 200 (2011).
[41]P. B. Changala, J. Chem. Phys. **140**, 024312 (2014).